European Journal of Neuroscience, Vol. 12, pp. 2608–2622, 2000

A quantitative study of gamma-band activity in human intracranial recordings triggered by visual stimuli

Jean-Philippe Lachaux,[1] Eugenio Rodriguez,[1] Jacques Martinerie,[1] Claude Adam,[1,2] Dominique Hasboun[1,3] and Francisco J. Varela[1]

[1]Laboratoire de Neurosciences Cognitives et Imagerie Cérébrale (LENA), CNRS UPR 640, Hôpital de La Salpêtrière, 47 Blvd de l'Hôpital,75651 Paris cedex 13, France
[2]Unité d'Epilepsie, Hôpital de La Salpêtrière, 47 Blvd de l'Hôpital,75651 Paris cedex 13, France
[3]Unité de Neuroradiologie, Hôpital de La Salpêtrière, 47 Blvd de l'Hôpital,75651 Paris cedex 13, France

Keywords: human, gamma-band activity, intracortical recordings, phase synchronization, surrogate data, time-frequency analysis, visual discrimination

Abstract

This paper studies gamma-band responses from two implanted epileptic patients during a simple visual discrimination task. Our main aim was to ascertain, in a reliable manner, whether evoked (stimulus-locked) and induced (triggered by, but not locked to, stimuli) responses are present in intracranial recordings. For this purpose, we introduce new methods adapted to detect the presence of gamma responses at this level of recording, intermediary between EEG-scalp and unicellular responses. The analysis relies on a trial-by-trial time–frequency analysis and on the use of surrogate data for statistical testing. We report that visual stimulation reliably elicits evoked and induced responses in human intracranial recordings. Induced intracranial gamma activity is significantly present in short oscillatory bursts (a few cycles) following visual stimulation. These responses are highly variable from trial to trial, beginning after 200 ms and lasting up to 500 ms. In contrast, intracranial-evoked gamma responses concentrate around 100 ms latencies corresponding to evoked responses observed on the scalp. We discuss our results in relation to scalp gamma response in a similar protocol [Tallon-Baudry *et al.* (1996) *J. Neurosci.*, **16**, 4240–4249] and draw some conclusions for bridging the gap between gamma oscillations observed on the scalp surface and their possible cortical sources.

Introduction

The purpose of this paper is to answer the following question. Can gamma band oscillatory activity concomitant to a discrimination task be reliably detected from signals from implanted electrodes in various sites of the human brain?

Oscillatory synchronization is being explored as a possible mechanism for the emergence of coherent neural assemblies underlying a number of perceptual, motor or cognitive behaviours (Freeman, 1975; Damasio, 1990; Abeles, 1991; Bressler, 1995; Singer & Gray, 1995; Varela, 1995). Much of the evidence rests on microelectrode recordings in awake animals finding millisecond-precise synchrony in spike firing, or between local field potentials (LFP) of multiunit recordings in the 30–70 gamma band (Gray *et al.*, 1989; Kreiter & Singer, 1992; Eckorn *et al.*, 1993; Neuenschwander *et al.*, 1996; Roelfsema *et al.*, 1997).

At the level of scalp-recorded EEG and/or MEG, evoked and induced gamma band emissions and synchrony concomitant to behavioural tasks have also been reported (Galambos *et al.*, 1981; Pantev *et al.*, 1991; Ribary *et al.*, 1991; Llinas & Ribary, 1993; Jokeit *et al.*, 1994; Pantev, 1995; Tallon *et al.*, 1995; Tallon-Baudry *et al.*, 1996, 1997; for review see Tallon-Baudry & Bertrand, 1999). For instance, Tallon-Baudry *et al.* (1996, 1997) carried out a trial-by-trial analysis of EEG responses in the gamma range following the presentation of coherent visual stimuli during a visual discrimination task. They found an early stimulus-locked ('evoked') component around 100 ms, and a later, stimulus-triggered ('induced') response with a peak at 280 ms.

To further study the origin, basis and operation of these gamma-band responses in humans, it is essential to provide links between the sources of such signals recorded from the scalp (EEG, MEG) and gamma synchronization effects observed from multiunit studies in animals. In the present study we profit from the unique opportunity afforded by the cooperation of epileptic patients implanted with multiple electrodes for preoperative focal localization to address these questions directly using a protocol comparable to that used on the human scalp. Such studies are surprisingly absent from the literature. Induced 40 Hz responses had already been observed intracranially following sensory stimulation in a pioneer study 40 years ago (Perez-Borja *et al.*, 1961). Menon *et al.* (1996) studied selective changes in spectral power during a sensorimotor discrimination task, but found surprisingly little evidence for specific spectral changes, and no evidence of coherence between sites separated beyond 2 cm. In contrast, in a recent study, Aoki *et al.* (1999) report very clear changes in the gamma band in adjacent sensorimotor areas during the performance of various visuomotor tasks. Our findings here on visual discrimination, confirm and complement theirs.

Thus our initial question can now be made more precise by restating it as two inter-related problems: (i) Does gamma band

Correspondence: Dr F. J. Varela, as above.
E-mail: fv@ccr.jussieu.fr

Received 28 October 1999, revised 8 March 2000, accepted 10 April 2000

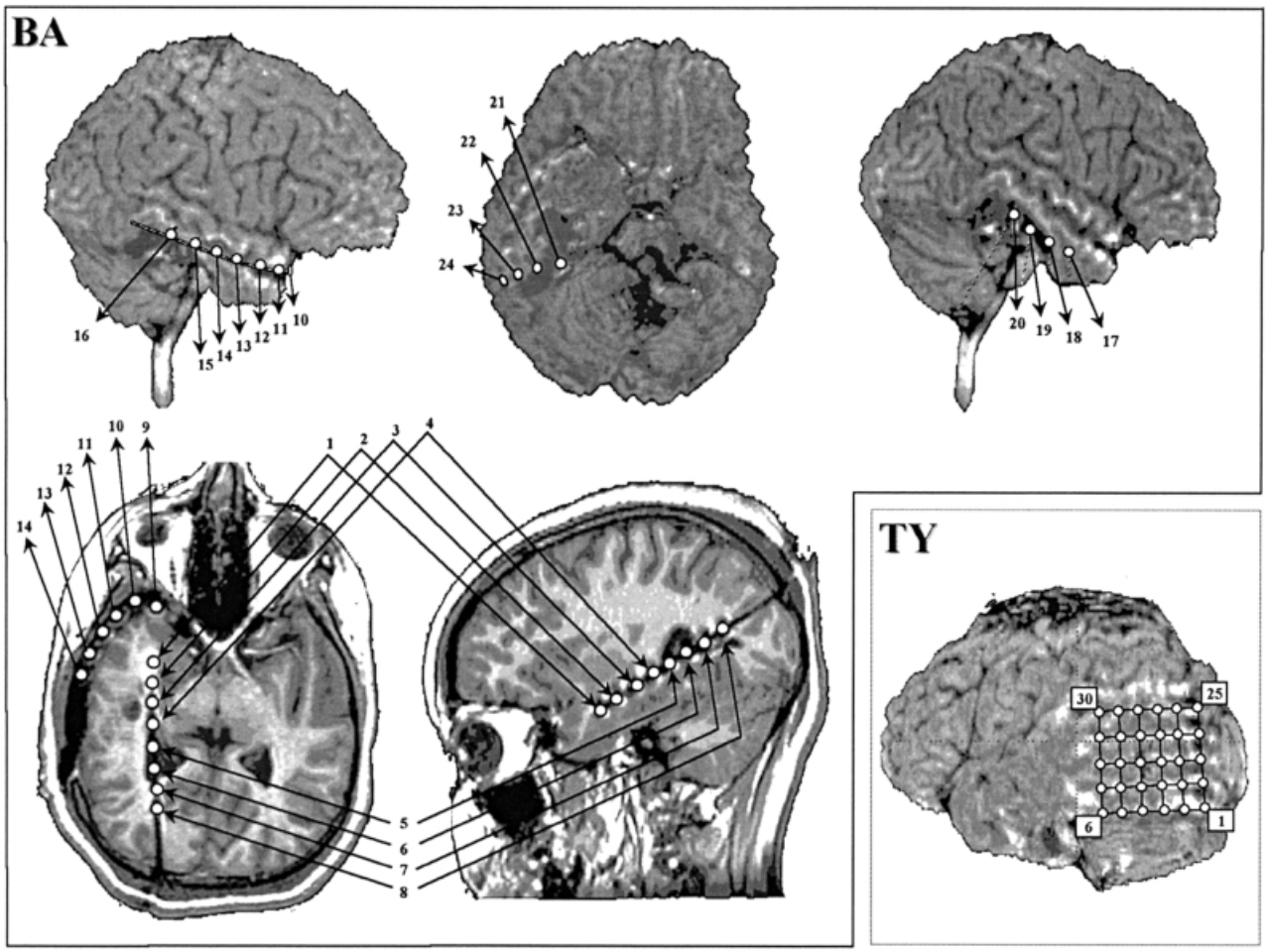

FIG. 1. Electrode locations based on postimplant MRI for subjects BA and TY. For anatomical precisions see Table 1.

activity measured in electrocorticograms follow reliably a discrimination task; and (ii) what are the methods needed to detect evoked and induced responses at this intermediate level of resolution? The further and essential question of whether such gamma-band oscillations enter into precise pair-wise synchrony over a short or large distance (i.e. > 2 cm) as a function of a cognitive task will not be addressed in this paper (but see Rodriguez *et al*., 1999).

Given that the electrodes used in this study were placed in preparation for a clinical intervention, and not for a neurocognitive study, and that our subjects were patients affected by a severe brain dysfunction, our main goal was not to focus on neurocognitive correlates of the discrimination tasks. Our emphasis throughout this paper will mostly be on the basic related question of whether gamma responses can be reliably detected in intracranial sites following perceptual stimuli, and, if so, whether electrocorticogram ECG recordings provide the source of gamma responses found in scalp studies.

Materials and methods

Patient profile and recording

We studied two subjects (one male, one female referred to below as TY and BA) suffering from intractable complex partial seizures. Their presurgical evaluation included simultaneous intracranial EEG and behavioural observation by video recordings.

TABLE 1. Patient BA: anatomical locations of the electrodes

Electrode	Location
1	Lateral part of amygdalan complex
2	Head of hippocampus
3	Head of hippocampus; in contact with lesion
4	Posterior part of hippocampus body
5	Tail of hippocampus
6	Junction between T4,O4, O5 and T5
7	Antecalcarine sulcus. Inferior part of parieto-occipital sulcus
8	Parieto-occipital sulcus
9	Right temporal pole (internal part)
10	Right temporal pole (anterior part)
11	Right temporal pole (lateral part
12	Parallel sulcus, junction between T1 and T2.
13	T1, slightly anterior to Heschl gyrus
14	T1, anterior part of Heschl gyrus
15	T1, Heschl gyrus
16	T2, posterior to Heschel gyrus, in proximity of plannum
17	T3
18	Junction between T3 and T2
19	Junction between T3 and T2; facing the lesion
20	T2, posterior part of Heschl gyrus, facing the lesion
21	Junction between T3 and T4. Close to lesion
22	T3, in contact with lesion
23	Low part of T2, close to T2/T3 junction
24	T2, Splenium, in contact with posterior part of lesion

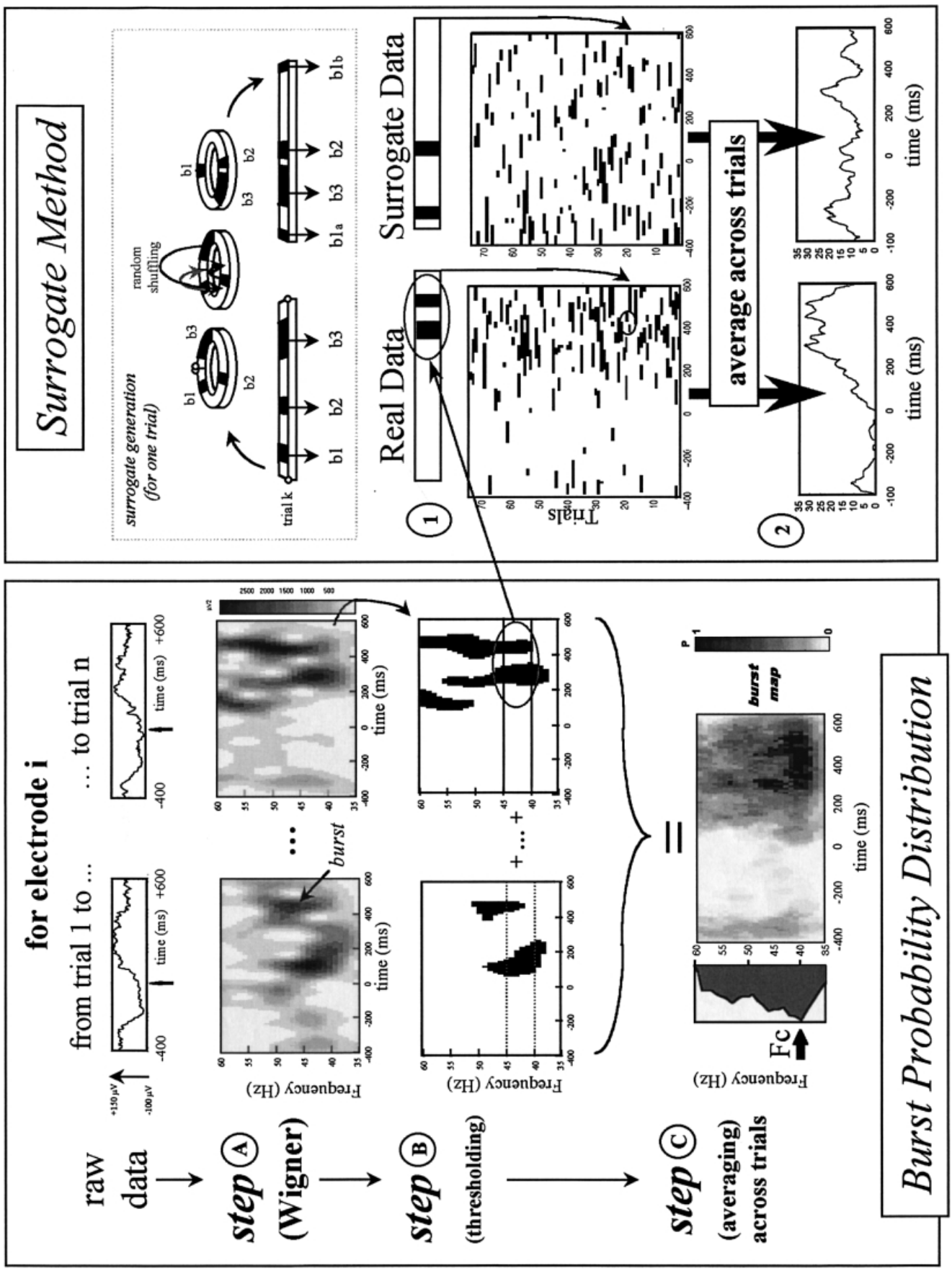
Surrogate Method
surrogate generation
(for one trial)
random
shuffling
trial k
b1
b2
b3
b1a
b1b
Real Data
Surrogate Data
Trials
average across trials
time (ms)
for electrode i
from trial 1 to ...
... to trial n
raw
data
step A
(Wigner)
step B
(thresholding)
step C
(averaging)
across trials
Frequency (Hz)
burst
msp
Fc
Burst Probability Distribution

TY

The first patient was a 23-year-old male whose ictal symptomatology, including visual hallucinations and speech disturbances, was suggestive of an epileptic focus of left temporo-occipital origin. A subdural grid with 30 contacts (6×5) separated by 1 cm was inserted into the convexity of the occipito-temporo-parietal cortex to better delineate the site of the seizure origin and to determine a functional map of language areas (Fig. 1). A continuous epileptic spike discharge was recorded under a single point of contact (No.9, see Fig. 1). Throughout the 4 days of preoperative monitoring, there was no spread to the adjacent contacts, suggesting a local focus of less than 1 cm^2. Using axial magnetic resonance imaging, contact no. 9 was determined to be at the junction between area 19 and infero-temporal cortex just beneath the lesion in an apparently healthy region. A subsequent lesionectomy including the pathological borders led to a seizure-free outcome for over a year. A meningo-angiostomosis was found under neuropathological examination.

BA

This young lady (18 years) was suffering from a pharmaco-resistant severe epilepsy for 3 years. Her initial symptom, a strong experiential phenomenon (an 'Eureka'-like impression) suggested the possibility of a neocortical temporal implication. The MRI showed a right basotemporal lesion that did not damage the mediotemporal structures (amygdalo–hippocampal complex). The intracranial exploration was aimed at delineating the epileptogenic zone, and in particular at verifying whether mediotemporal structures participate in the initial ictal onset. Thus, an intracranial electrode with 8 contact points and 3 subdural strips (1×8 contacts plus 2×4 contacts) were implanted stereotaxically under MRI control (Fig. 1). Most of the recorded seizures came from the area of the lesion. After lesionectomy (showing a dysembryoplastic neuroepithelial tumour at neuropathology) the patient has been seizure-free for over 2 years (Table 1).

Signals from the recording sites and an electro-oculogram were simultaneously recorded with an external linked ears reference, amplified, filtered using a 0.08–100 Hz bandpass filter, and digitized at 1 kHz. Over 1 h of recording was transferred to a magneto-optical media for off-line analysis. Stimulation and motor responses were all under a computer-controlled acquisition program.

Stimuli

Following written informed consent from the subjects, recordings were taken in blocks comprising three consecutive experimental conditions: (a) a period of passive visual fixation lasting 500 s; (b) a visual discrimination task involving a finger response; and (c), a hyperventilation condition lasting 140 s. The subject was seated in a recording chamber under scotopic conditions in front of a stimulation screen, and fitted with an acoustic headset. S/he was allowed time to become accustomed to the environment, and was accompanied at all times by a physician. The entire procedure lasted 1 h including rests between experimental blocks.

In the discrimination task, referred to as the Kanizsa task, three types of visual stimuli were delivered: an illusory triangle (Kanizsa, 1976; 160 presentations), a real triangle (160 presentations) and an inside-out Kanizsa triangle (80 presentations; see Fig. 7 for illustrations). The stimulations were presented in a random order, and lasted 40 ms. The subjects pressed a button with the right hand each time s/he detected the inside-out Kanizsa triangle. Inter-stimulus interval varied randomly between 800 ms and 1200 ms. This Kanizsa task is a simplified version of an original protocol used by Tallon-Baudry *et al.* (1996), where a curved Kanizsa triangle was interleaved with the other stimuli to keep the subject's focus on the illusory contours of the Kanizsa triangles. Although this original protocol may be better suited to study the cognitive aspect of gamma responses, it induced an additional degree of difficulty that proved to be too demanding for epileptic patients.

Time-frequency analysis of the signal

Analysis of energy emission

The procedure used here to analyse energy emissions in the electrocorticogram was designed to fit two remarkable properties of our intracortical recordings: (i) for each trial, the energy of the recordings above 10 Hz was concentrated around specific latencies and frequencies. We called these regions of high energy 'time-frequency bursts' (Fig. 2); and (ii), the exact latencies of these bursts was highly variable from trial to trial, reminiscent of the variability seen in oscillatory bursts in local field potentials recorded from a small number of units in animals (see, e.g. Kreiter & Singer, 1992; Neuenschwander & Varela, 1993). In this procedure, we considered the burst latencies in individual trials as random variables and estimated their statistical distribution. We specifically addressed the question of whether these bursts were pure spontaneous activity (flat distribution) or whether their statistical distribution was affected by visual stimulations (peaks of the distribution at specific latencies).

The analysis consisted of two major parts (see Fig. 2): (i) the construction of maps that indicate the probability of occurrence of bursts in time and frequency; and (ii), a statistical analysis that detects whether bursts tend to accumulate at specific latencies. The statistical analysis requires that we focus on a narrow frequency range (bandwidth of 5 Hz), which means that it must be repeated over several chosen frequencies to cover the entire response range. An exhaustive study of the entire broad frequency range in intracranial responses is beyond the scope of this paper which aims at demonstrating the feasibility of the analysis and at showing several characteristics of intracranial gamma activity. Thus, we have focused on a specific band in the gamma range (40–45 Hz), which illustrated clearly the main claims of this paper. It is also a frequency where the

FIG. 2. Analysis of the energy emission for one electrode. Left panel, computation of the burst probability distribution. For each trial, the raw data are filtered (high-pass filter at 35 Hz, not shown) and their time-frequency map (pseudo Wigner–Ville transform) is computed (step A). The energy is restricted to small regions of the time-frequency domain in time-frequency bursts. Next, these maps are thresholded (step B) and the digitized outputs are averaged across the trials (step C). The result of this procedure is a burst probability distribution. Summing over columns yields a frequency histogram; Fc indicates the frequency chosen for subsequent analysis in this study. Right panel, surrogate method for the estimation of significant energy increases. A narrow slice of the digitized Wigner–Ville maps (red arrow) provides for each trial a binary function (1), which indicates the latencies of the bursts around frequency Fc ($\pm$ 2 Hz). A 'burst-matrix' is then constructed from the entire array of such single trial binary functions; the sum of its rows gives a time burst function (2). This function gives the proportion of trials for which a burst is present around Fc $\pm$ 2 Hz. Similarly, surrogate time burst functions are computed from a surrogate burst matrix. These surrogate burst matrix are generated as follows (top inset). For each trial, the binary function obtained from thresholded Wigner–Ville maps is made of blocks of 1 (black boxes) and 0 s (blank spaces) of various lengths. These blocks are shuffled at random latencies (but preventing blocks to overlap); when a block is placed at the end of the time window, it is cyclically continued at the beginning (periodic boundaries, observe block b1).

most salient response is found. The reader should be aware that the phenomena we describe hereafter are probably not specific to this narrow range, but it occurs, with varying amplitudes and latencies in a wider frequency range (Fig. 6).

Construction of time-frequency burst probability maps

The first part of our procedure estimates the bursts' statistical distribution. As is already established, mesotopic electrical neuronal responses roughly follow a 1/f distribution. Accordingly, to minimize interference due to the relatively high amplitude of lower frequency bands (1–20 Hz), and thus to allow the detection of low-amplitude, high frequency emissions all the signals were first high-pass-filtered with a low cutoff at 35 Hz (the filter had a finite impulse response of 256 ms). This high cut-off frequency follows from our choice to study frequencies above 40 Hz; a 35-Hz cut-off suits the study of all frequencies higher than 40 Hz, for reasons detailed in step B.

Step A

After filtering, we applied to each trial a smoothed-pseudo-Wigner–Ville transform (Fig. 2, left panel) to compute the energy (PWV(f,t))

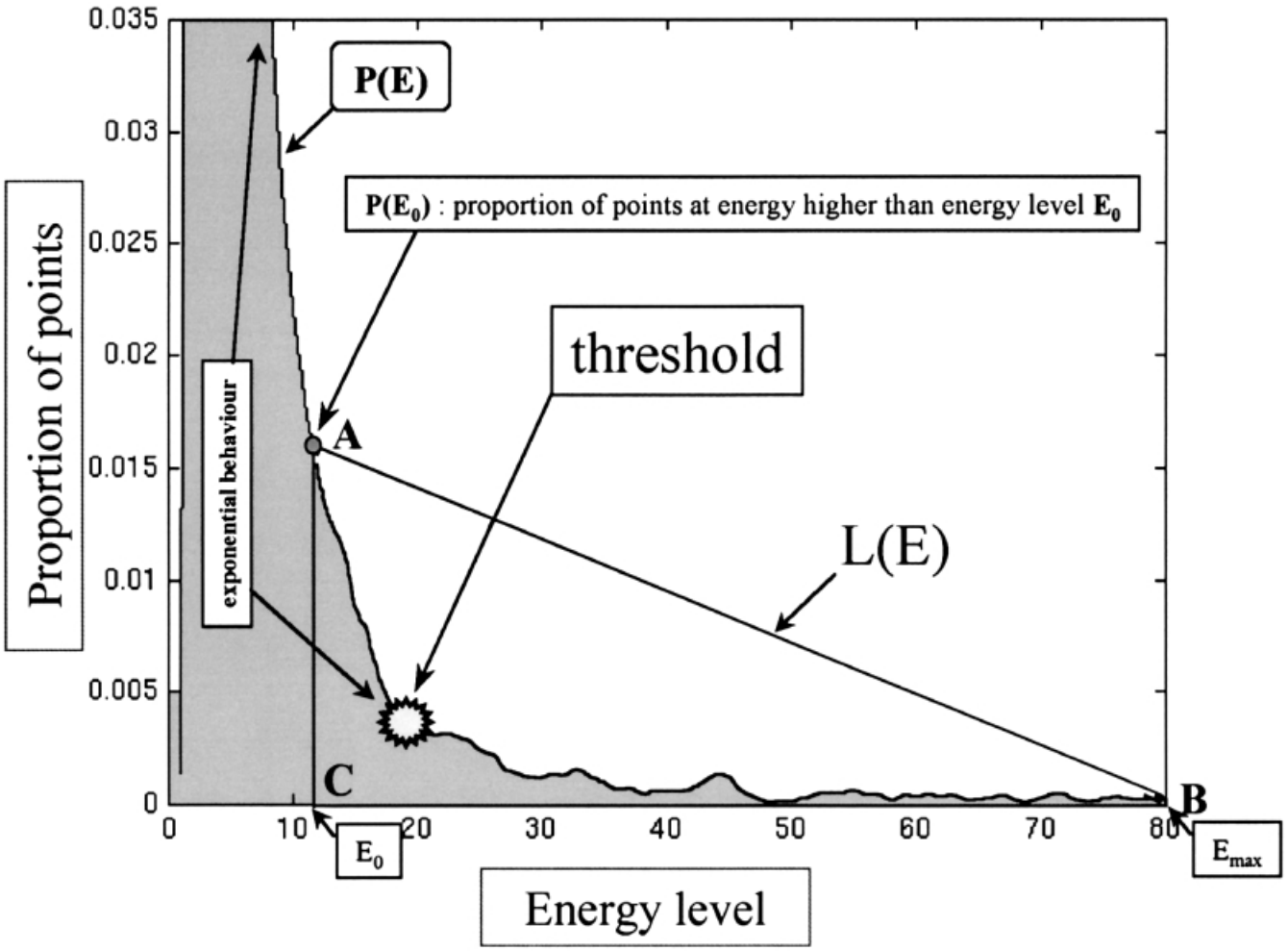

FIG. 3. Description of the thresholding method. From the Wigner–Ville map of a signal (one electrode, one trial), we compute a function P(E), which is the proportion of time-frequency points in the map with an energy higher than E, for E between 0 and the maximum value of the energy map E_{max}. P(E) always decreases exponentially. For every energy value Eo, L(E) is the function decreasing linearly from P(E) to 0 in the interval [E,Emax]. A $\{E_0,p(E_0)\}$, B (Emax, 0) and C (E_0,0) define a triangle which surface is the integral of L(E) between Eo and Emax. See text for the description of the threshold selection.

FIG. 4. Analysis of the phase alignment for one electrode. (a) For each trial, the raw data were band-pass filtered (40–45 Hz). (b) From the resulting oscillatory signal we extracted a binary function of time: 1 when the oscillation reached a maximum and zero elsewhere. (c) From the binary functions for all the trials, we computed, by step 1 and 2 (Fig. 2), a matrix (called a 'phase-matrix', the columns of which were summed to provide a mean-phase function. (d) The phase function oscillated (at 43 Hz) when the phases of the trials were aligned (circled portion). The Wigner–Ville transformation of the mean-phase function provided a map in which energy was concentrated around 43 Hz. The phase alignment function was defined as the energy of this map at 43 Hz. (e) The phase alignment function reached high-values when the maxima of all single trials were aligned. Following the same procedure, phase alignment functions were also computed for surrogate phase-matrix. (c, right) The surrogate phase matrixes were generated by random time-translations of the rows of the original phase matrix. The value at time t became the value at time (t-τ) modulo the length of the time interval, where τ was randomly chosen between –1/43 s and 1/43 s, different on every trial. This procedure broke all possible phase-alignments due to the stimulation.

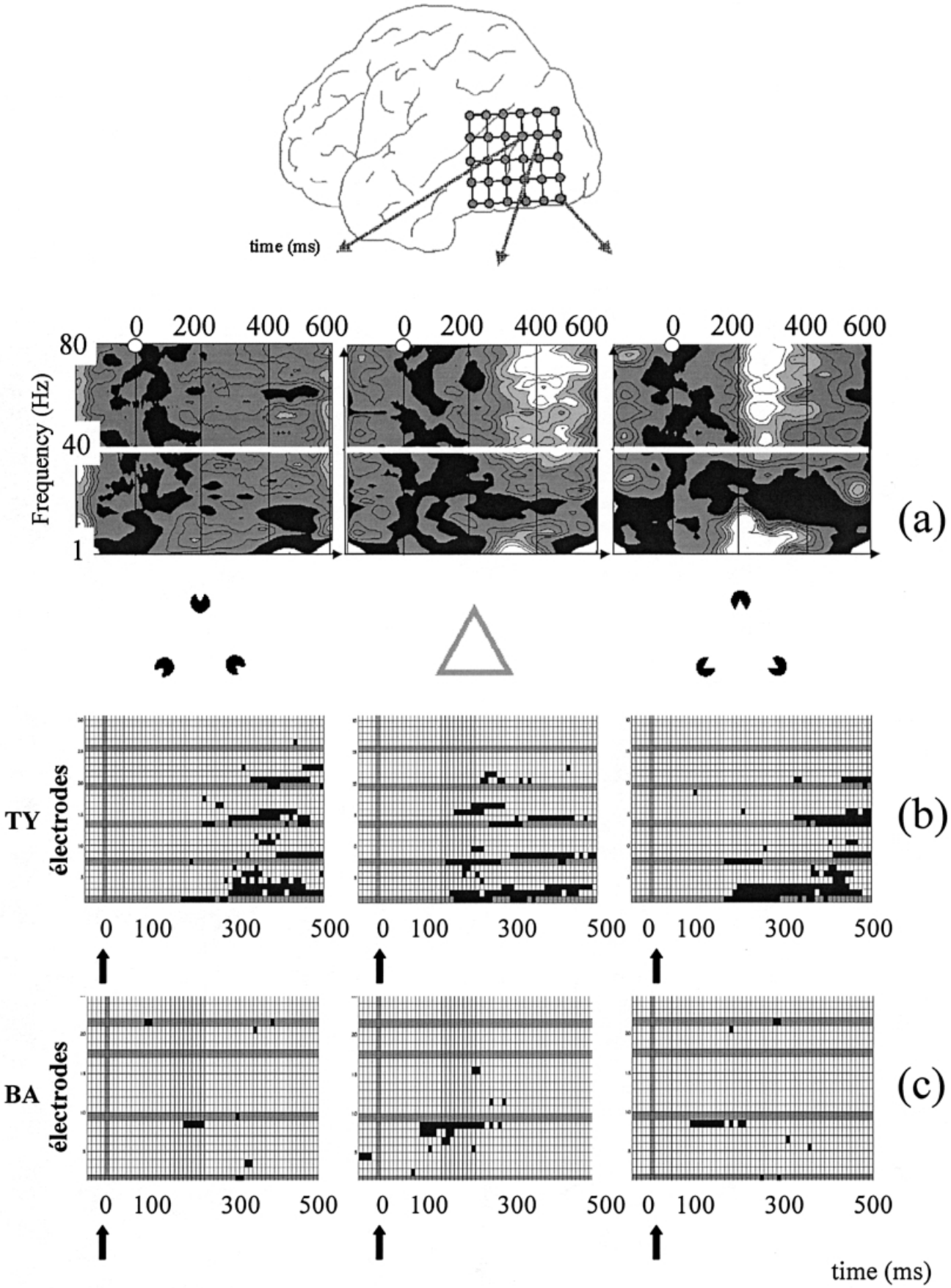
time (ms)
0 200 400 600
0 200 400 600
0 200 400 600
80
40
1
Frequency (Hz)
(a)
TY
électrodes
(b)
0 100 300 500
0 100 300 500
0 100 300 500
BA
électrodes
(c)
0 100 300 500
0 100 300 500
0 100 300 500
time (ms)

present in the electrocorticogram at each frequency, f (between 35 and 100 Hz) and each latency t, (between 400 ms before the stimulation and 600 ms after; see technical appendix for the formula and some details of the smoothed-pseudo-Wigner–Ville transform). As mentioned above, these time-frequency maps were sparse; the main part of the energy was contained within narrow regions (the time-frequency bursts); and the latencies of these bursts were highly variable from trial to trial.□

Step B

In each map, bursts were identified using a digitalization process (Fig. 2, left panel) carried out by thresholding the Wigner–Ville map with an adaptative thresholding procedure; when Wigner maps are thought of as landscapes, electrocorticogram Wigner maps look like isolated peaks in a flat valley. The purpose of the thresholding procedure is to identify those peaks, or bursts. For each map, it sets a threshold defined as the lowest energy level (or 'altitude') above which only peaks emerge. Specifically, as described in Fig. 3, for each energy level, E we measure the surface of the map lying above that level, P(E). As E increases, the background activity of the valley sinks rapidly under the rising energy level E and the slope of P(E) is high, P(E) decreasing exponentially. Eventually, E reaches a critical value above which only bursts emerge. This critical value is the selected threshold, E_o. Above that threshold, the decrease of P(E) is much slower, until all peaks eventually disappear when E goes beyond the maximum energy of the map, E_{max}. The threshold is found following the geometrical procedure just described (Fig. 3); for each energy level E_o, this procedure compares P(E) on the interval $[E_o, E_{max}]$, with a function decreasing linearly from $P(E_o)$ to zero (L(E)). The idea is that the relative difference between these functions drops sharply at the end of the initial exponential phase of P(E). The relative difference between P(E) and L(E) is computed as follows.

$$\int_{E_0}^{E_{max}} |P(E) - L(E)|dE / \int_{E_0}^{E_{max}} |L(E)|dE. \quad (1)$$

In Fig. 3, this is the ratio of the surface of the white part of triangle ABC divided by the total surface of triangle ABC. The lowest energy value for which this difference reaches a local minimum is chosen as the threshold. A new threshold value is computed for every electrode and trial.

This digitalization transforms each Wigner–Ville map into a binary map, segmenting the time-frequency regions in which bursts occurred (energy set to 1) against a surround (set to 0). It is here that the rationale for high-pass filtering the data prior to the analysis as discussed before appears most clearly. As the energies above 35–40 Hz were much smaller compared to the components at lower frequencies (i.e. a 1/f specturm, without filtering, these low-frequency would have masked the high-frequencies in the thresholding procedure by setting the threshold to a very high value, making the analysis of high-frequency emisions impossible. The lower and higher bands must be studied successively.

Step C

Finally, binary maps were averaged across trials to yield a time-frequency burst-probability maps (Fig. 2, left panel), which values indicate the proportion of trials for which a burst occurred at a given time-frequency location. With an infinite number of trials, these probability maps would be flat except if visual stimulations affect the bursts' production. In real cases, however, spurious peaks, not due to the stimulations, are present in the maps because the number of trials is finite. The second part of the analysis discriminates between the spurious peaks and actual effects of the stimulations (Fig. 3).

Determining whether time-frequency bursts were stimulus-induced.

For each peak of a time-frequency burst-probability map we tested the H_0 hypothesis that the peak was not due to an actual maximum; but appeared only because the number of trials is finite. The statistical test developed here applies only to narrow frequency ranges. For reasons already discussed, this study focuses on the 40–45 Hz frequency range. A preliminary analysis of all frequency ranges (see examples in Fig. 6) revealed significant results at other frequencies. The choice of this specific range was motivated by its central location in the gamma band, its clear separation from the A/C noise component at 50 Hz, and the strength of the effects observed.

H_0 was tested by comparing the burst probability maps obtained for the original data and for a set of 200 surrogates (Theiler *et al*., 1992). Surrogate probability maps were created from the original data following the same steps (A–C), plus a shuffling procedure between steps B and C. Independently for each trial, bursts occurring in the 40–45 Hz range were repositioned at random latencies (as shown in Fig. 2; periodic boundary conditions and no overlap between bursts). This procedure aimed at breaking any effect of the stimulations on the latencies of bursts in the surrogate. A peak in the original burst probability map was considered significant (indicating a effect of the stimulation) when less than 5% of the surrogate data could reach a value that high (at any latency).

This analysis is meant to be repeated for several frequencies, in order to cover a broad frequency range. However, when analysing N frequency bands with a statistical threshold p, one should be careful at the end of the process, that the probability of having incorrectly rejected the H_0 hypothesis for one of the bands is Nxp. Therefore, it is advisable to chose N and p such that $Nxp < 5\%$.

Also, as time-frequency estimation is not completely independent from one band to the next, independent tests can only be carried in frequency bands separated by more than the temporal resolution of the smoothed-pseudo-Wigner–Ville transform. With smoothing windows of 128 ms and a sampling frequency of 1000 Hz, this temporal resolution was between 10 and 15 Hz, and 8–10 tests are sufficient to study a broad (1–100 Hz) range (Fig. 4).

Analysis of evoked responses

A second surrogate-based procedure was introduced to test for the presence of responses time-locked to the stimulations. For each trial, signals were band-pass filtered to extract their oscillatory component

FIG. 5. Induced responses in subdural recordings. (a) This panel shows the induced response for the entire frequency range (1–80 Hz) in three representative electrodes of subject TY during the Kanizsa task. The left and middle maps correspond to two electrodes separated by the temporo-occipital junction. These maps were obtained using a procedure described in Appendix II. In contrast with scalp results, the strength of induced responses, depend on electrode position. High-frequency induced responses appeared at frequencies higher than 35 Hz, while energy between 15 and 35 Hz was virtually unchanged by stimulation. (b) Subject TY, significant induced responses ($P < 0.05\%$ that the null-hypothesis is true) for all electrodes and in the chosen gamma range (40–45 Hz), following the procedure introduced here (see Methods). Each row of the matrix corresponds to one electrode from the cortical grid (Fig. 1). Grey lines indicate electrodes (1, 7, 13, 19, 25) and serve as visual aids to identify successive rows of electrodes. (c) Subject BA, same conventions as in (b) for patient BA.

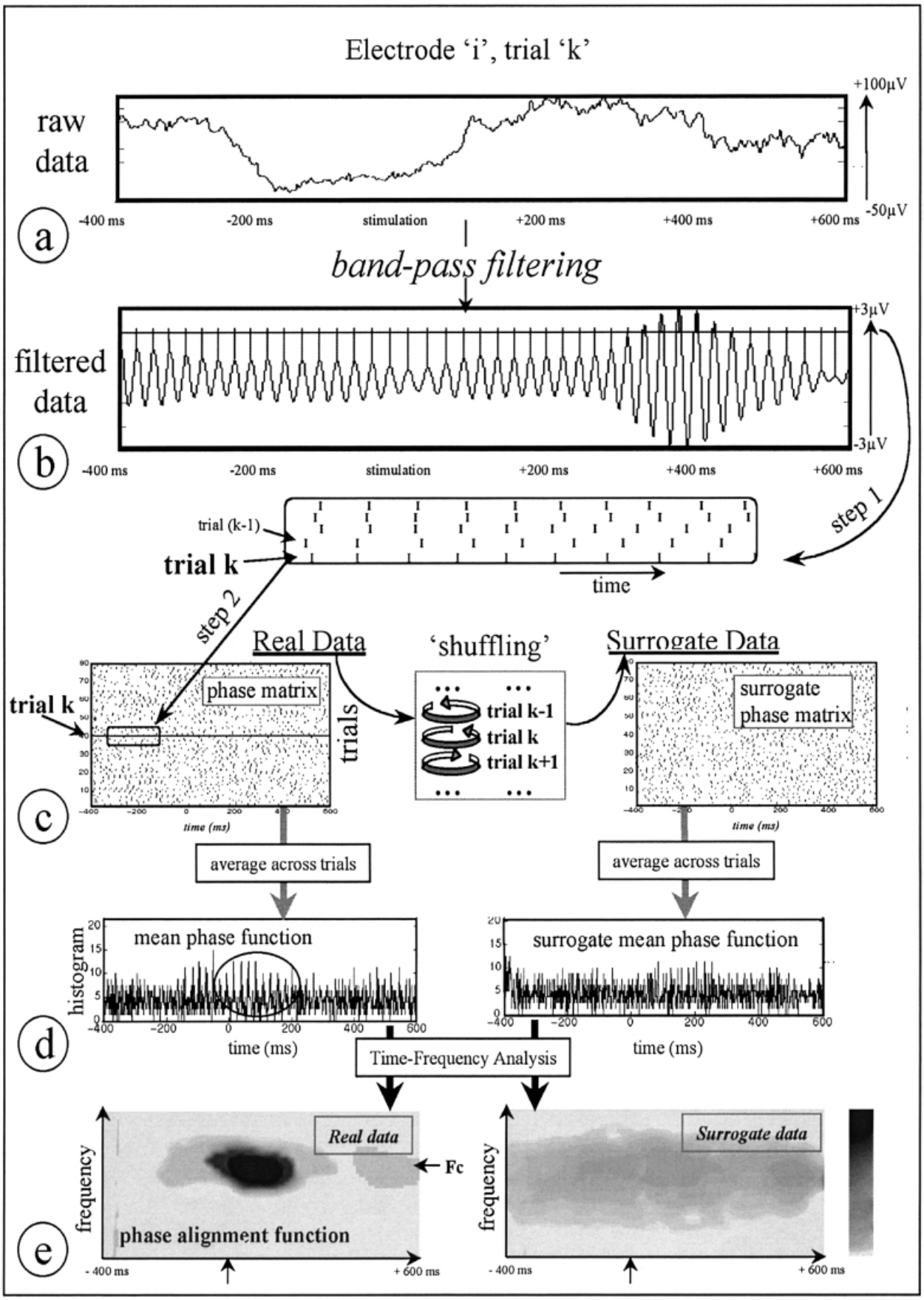
Electrode 'i', trial 'k'
raw data
+100μV
-50μV
-400 ms
-200 ms
stimulation
+200 ms
+400 ms
+600 ms
a
band-pass filtering
filtered data
+3μV
-3μV
b
step 1
trial (k-1)
trial k
time
step 2
Real Data
'shuffling'
Surrogate Data
phase matrix
trial k
trials
trial k-1
trial k
trial k+1
surrogate phase matrix
time (ms)
c
average across trials
average across trials
mean phase function
surrogate mean phase function
histogram
time (ms)
d
Time-Frequency Analysis
Real data
Fc
Surrogate data
frequency
phase alignment function
- 400 ms
+ 600 ms
e

in the 40–45 Hz range. These filtered signals were then converted into spike-trains, each spike indicating the latency of a local maximum (Fig. 4a and b). The average of these spike-trains across trials (Fig. 4c and d) is a continuous function of time reaching values between 0 and 1. A value of 1 indicates that at this time, the phase was the same for all trials. The Wigner–Ville transform of this function (called phase-alignment function) further quantifies the degree of phase-alignment across the trials (Fig. 4e; note here that as the signal has been filtered, its time-frequency energy is necessarily restricted around 43 Hz, and the Wigner of the phase-alignment function is equivalent to the extraction of its envelope).

For each peak of the phase-alignment function, we used surrogate data to test the H_0 hypothesis that the peak was not due to an effect of the stimulation on the phase alignment of the trials, but appeared solely because the number of trials was insufficient. Surrogate alignment functions were obtained by averaging the spike-trains of the original data, after translating each of them in time independently of each other. The lag was randomly chosen for each trial between [1/43Hz (–23 ms), 1/43Hz (+23 ms)] so as to break all possible time-locking due to the stimulation (Fig. 4d and e). For each peak of the original alignment-function, we calculated the proportion Ps of 200 surrogate alignment functions that reached values higher than this peak. This bootstrap method measured the risk of rejecting the null-hypothesis H_o. Phase-locking was considered significant when this risk was less than 5%. As the previous statistical analysis, this test is meant to be repeated over several frequency ranges., with the same requirements imposed by this repetition.

This method represents an alternative approach to that introduced by Tallon-Baudry *et al*. (1996, 1997) to efficiently remove the effect of intertrial amplitude modulations and estimate the stability of the phase of EEG signals across trials. That method estimated the instantaneous phase of the signals using a wavelet transform and the degree of phase-locking using a Raleigh test. However, the definition and estimation of the instantaneous phase of EEG signals in a precise frequency range is not straightforward (Lachaux *et al*., 1999). We favoured here the measure of the latencies of the maxima of the band-pass filtered signal, as the most direct measure of the instantaneous phase.

Results

Following the analysis presented above, we have studied the effects of visual stimulations on the subdural gamma activities for patients TY and BA performing the Kanizsa visual task (Figs 5–7). We first present the induced gamma emissions (analysis of energy), then the evoked gamma responses (phase-locked to the stimulation).

Induced gamma emission analysis

The grid of electrodes implanted in patient TY gave us access to a portion of cortical surface surrounding the left temporo-occipital junction (Fig. 1). Time-frequency analysis showed that the gamma activity was characterized in this region by patterns of transient oscillatory bursts (usually shorter than 200 ms), for which latencies were highly variable from trial to trial. The time-frequency chart for a broad frequency range (1–80 Hz) for three electrodes is given on Fig. 5a. They provide a striking illustration of latency variability and their regional specificity in gamma responses. Two adjacent electrodes (20 and 21), both located on the occipital lobe and separated by only 1 cm on the cortex surface, had opposite types of emission: fully active in one, almost flat on the adjacent one. In contrast, electrode 1 does reach high values of induced activity but they are significantly time-shifted from 400 ms (electrode 20) to 250 ms.

The surrogate procedure described above allows us now to determine whether, in spite of such variability, the induced responses were significantly related to the visual task. (Fig. 5b) shows the induced activity over all electrodes which are significant at a 0.05 level and only in the 40–45 Hz range (black squares indicates a significant time bin). It is clear that bursts were more likely to occur after the stimulus only, and in a spread of latencies between 150 and 500. The precise timing varied with electrode position. Some electrodes had rather early effects, starting as early as 150 ms after stimulation and ending before 400 ms (electrode 1 for instance), while other had much later effects (such as electrode 8). It is also clear that the effect of stimulation in the gamma-band was quite localized in space; they are concentrated especially on the occipital side of the temporo-occipital junction (cf. electrodes 1–3, 7, 8, 13, 14).

The three component stimuli of the visual task generated comparable patterns of induced activity (Fig. 5), and it does not seem possible to separate target and nontarget responses. However a detailed observation does reveal some differences for each electrode between the peak latencies produced by the three stimulations. Electrode 10 for instance only responds to everted circles. In addition, the region of electrodes 14–15 seems to respond with a significantly later delay (around 500 msec) in the target stimuli, but respond actively around 350 msec for the nontargets. A full study of the exact influence of stimulus shape on the spatio-temporal organization of gamma energy increases was unfortunately beyond the reach of this study, since it would have required several subjects with similar implanted electrodes.

Results for patient, BA, reproduced the main effects observed in TY, but more sparsely. Namely, our analysis also revealed that the stimulations induced significant peaks in burst distribution (Fig. 5c), and these effects were found in several locations with dissimilar probability. The main effects were also found in the occipital cortex, like the antecalcarine sulcus (electrode 7) and the parieto-occipital sulcus (electrode 8). However, BA's more extended implantation revealed that visual stimulations also induced responses in other cortical regions, namely the temporal lobe (electrodes 11, 15, 20 and 21) as well as in subcortical regions, in the amygdalo-hippocampus complex (electrodes 1–3). Responses occurred in BA earlier than for TY (no later than 350 ms) and mostly between the 100 and 200 ms range. We had no means to ascertain whether such differences are due to electrode location or individual differences.

FIG. 6. Responses induced by the target stimuli at various frequencies. This figure shows, for both subjects, the latencies and electrodes where bursts accumulated following target stimuli at various distinct frequencies. Same convention as in Fig. 5. Stimuli induced significant responses in a wide frequency range. Early induced responses were observed mostly at low frequencies. Responses at 23 Hz were obtained by high-pass filtering the data at 20 Hz, instead of 35 Hz. A 30 Hz cut-off frequency was used to study frequencies around 33 Hz. Other frequencies (43, 53 and 63 Hz) were analysed after high-pass filtering at 35 Hz. Bottom: normalized power spectrum of the electrocorticogram signals averaged over all electrodes and stimuli for TY (left) and BA (right). The power is proportional to the inverse of the frequency. Power above 30 Hz is only a fraction of the power below 30 Hz.

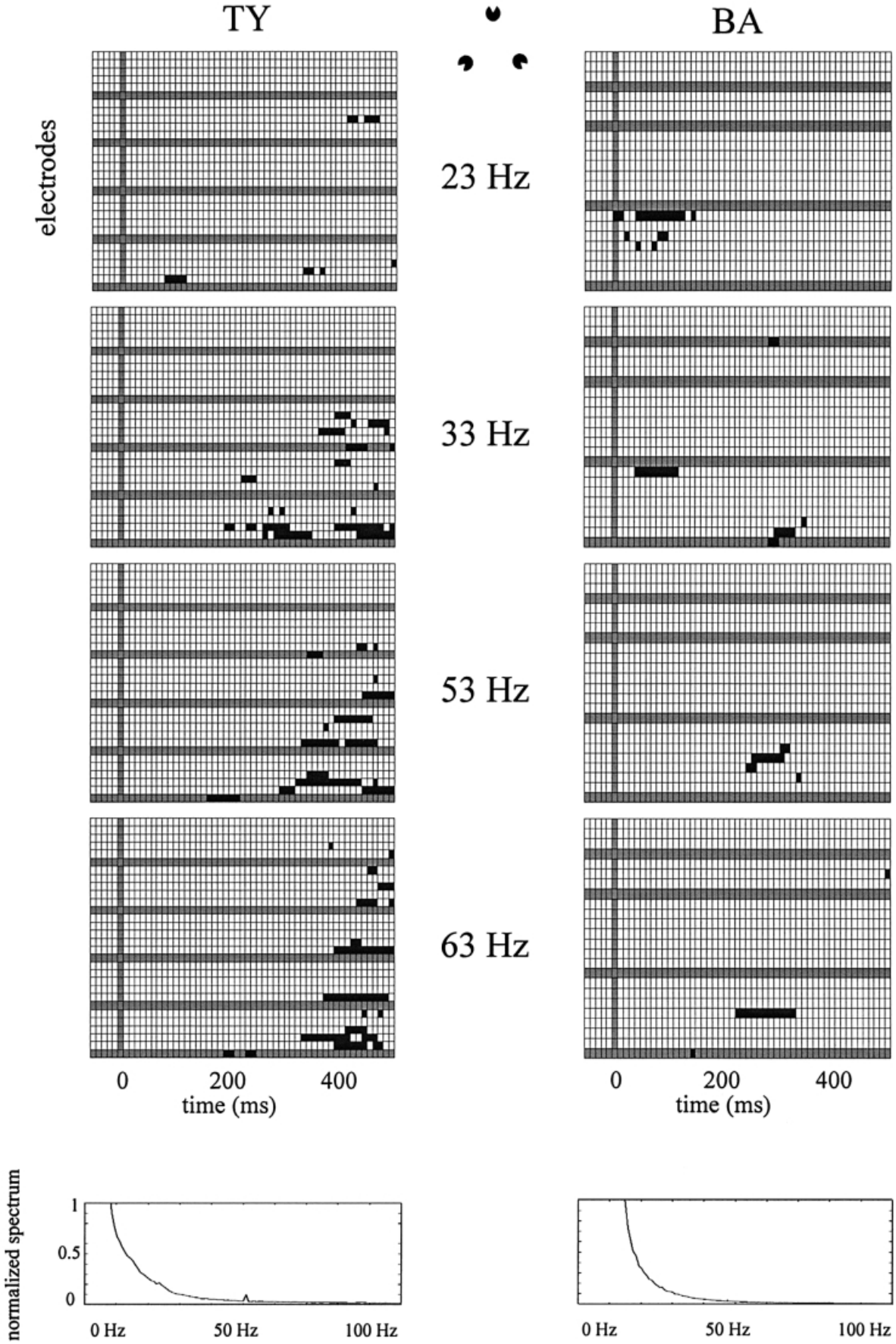
TY
BA
electrodes
23 Hz
33 Hz
53 Hz
63 Hz
0
200
400
time (ms)
0
200
400
time (ms)
normalized spectrum
1
0.5
0
0 Hz
50 Hz
100 Hz
0 Hz
50 Hz
100 Hz

Evoked gamma emission analysis

The application of the second algorithm described in the 40–45 Hz range gave us the evoked responses for both patients (Fig. 7). This figures shows both the gamma event related potential (Fig. 7a and b), and the significant periods of phase alignment at the 0.05 level (Fig. 7c).

For subject TY the evoked responses are concentrated on the occipital side of the grid (electrodes 2, 7, 13, 14, 19), showing early gamma oscillations that are phase-locked to the stimulus within the first 100 ms following stimulus onset. When averaging across the trials, oscillations aligned in phase over trials add to each other to create a characteristic peak in the average signal: the evoked gamma response, or gamma event-related potential (GERP). These GERPs are seen in Fig. 7a and b, as raw averages, and normalized for each individual electrode for ease of comparison. By construction, the phase of the gamma evoked response matches the phase that repeats across trials among the phase-locked gamma oscillations. This phase is an important cue for the origin of these responses. For instance there is a clear phase difference between the evoked responses of electrode 2 and 7, indicating, perhaps, two different neuronal ensembles as source. Interestingly, the phase of the evoked response for each electrode remained remarkably constant across conditions.

Significant phase-alignments (at the 0.05 level) all coincide with the GERPs early latencies. Note that phase-alignments seem to appear before the stimulation. This is due to an inevitable loss of temporal resolution introduced by the filtering step; any time-frequency analysis necessarily yields effects shortly before the stimulation when strong oscillations start at very early latencies.

Thus although induced and evoked responses gathered on the occipito-temporal junction, the two responses could easily be separated. While induced responses emerged at latencies later than 150 ms, evoked effects occurred earlier, shortly after the stimulation and did not last after 200 ms. Also, if some electrodes with evoked effects also showed and induce response, the opposite was not always true. For instance, electrode 1 had a substantial induced, but no evoked response. Therefore, phase and energy modifications corresponded to two distinct phenomena, likely to reflect two different stages of visual process.

Concerning BA, evoked responses also corresponded well to those found in patient TY. These responses are at early latencies (within the first 100 ms following the stimulation) and last for the same stretch over 100–200 ms. They can be detected primarily from cortical areas adjacent to the occipital cortex (electrode 6 and 8), but seem to extend to a subcortical region identified as the tail of the hippocampus (electrode 5).

Discussion

Main results

The results just presented provide several hitherto unknown important characteristics of human intracranial gamma activity, even though we have concentrated in the specific 45 Hz range: (i) human intracranial induced gamma activity appears in brief bursts of about 200 ms; (ii) the time distribution of these bursts relative to stimulus arrival is highly variable from trial to trial, and differentially distributed in specific cortical and subcortical regions (temporo-occipital cortex, amigdalo-hyppocampal complex); (iii) these latencies can vary dramatically across the cortical surface over distances as short as 1 cm; (iv) there are evoked (phase-locked) subdural and subcortical regions where bursts are observed (the phase of these responses is specific to their anatomical origin, and remains constant across stimulations types); and (v), these evoked responses appear at early latencies, within 150 ms following the stimulation.

Methodological aspects

This study introduces two methods specifically designed to reliably detect evoked and induced gamma-band response in intracortical recordings of the human brain following perceptual stimulation. We based our analysis on the observation that gamma energy appeared at this level by bursts, well-located in the time-frequency domain but highly variable across trials, and therefore we focused on the statistical distribution of these bursts. This method differs from the only other procedure used to detect induced responses at the scalp's surface, which consists in averaging the time-frequency maps of the signals across trials (e.g. Tallon-Baudry *et al*., 1997). These two approaches are, in some senses, complementary. The burst detection method is best used where there is a large variability in the responses, as is the case in intracortical recordings. In scalp data, averaging the time-frequency maps still allows to find the frequencies where visual stimulations generate the strongest responses. These frequencies can then be the targets to more-detailed analysis based on bursts detection. In fact the main advantage of the burst detection is that it provides a detailed description of the considerable variability in the timing of the gamma responses. This variability should not be considered as noise to be eliminated by averaging techniques, but as an intrinsic property of ongoing significance (cf. Arieli *et al*., 1996; Ferster, 1996). The burst detection gives access to the full distribution of the bursts, and not only to its first moment, the average across trials. Furthermore, such a probability-orientated technique prevents epochs with very large peaks to be over-represented in the final estimation. Also, it allows a surrogate-based statistical analysis to estimate for one single subject if energy peaks of the distribution were really due to the stimulation.

Bridging levels between multiunit and scalp recordings

In a visual discrimination task presenting similar stimuli, neural activity carrying functional but with a more elaborated protocol focusing the subjects attention on the illusory contours of the Kanizsa triangle (Tallon-Baudry *et al*. (1996) first described that stimulations generated two kinds of responses in the EEG of normal subjects in the gamma range: an early (around 90 ms) evoked component, and a later one induced one (between 200 ms and 400 ms). These authors questioned whether their results could be related to gamma oscillations obtained at the multiunit level in the anaesthetized cat by Gray *et al*. (1989), and presumably involved in neural integration. This question is difficult to answer because of the relatively small amount of human data at intermediate level of resolution between MUA and EEG (Schürman *et al*., 1997).

FIG. 7. Evoked responses in subdural recordings. (a) Average responses in the chosen frequency (45 Hz), that is, the gamma event-related potentials (GERP) for all electrodes for the Kanizsa task in patient TY. Conventions as in Fig. 5. A GERP of large amplitude is visible in the occipital regions. (b) Same data as in (a), but the values for each individual electrode have been normalized showing that the evoked gamma responses is present over all electrodes at a stable latency (around 100 ms), in spite of amplitude differences. (c) Chart of significant phase-locking responses calculated according to the procedure introduced here. After surrogate testing ($P < 0.05\%$ that the null-hypothesis is true) only few electrodes are active.

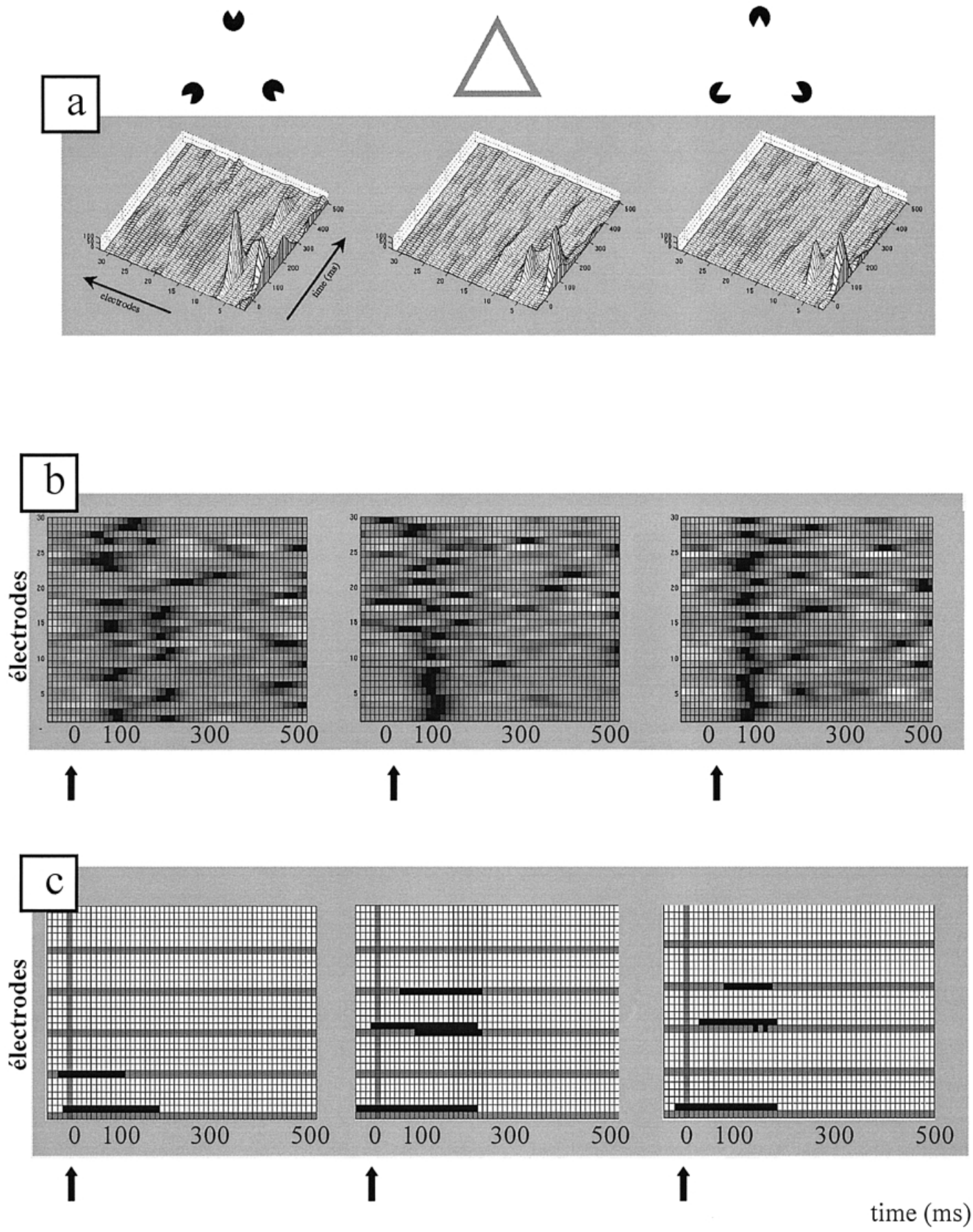
a
electrodes
time (ms)
b
électrodes
0 100 300 500
c
électrodes
0 100 300 500
time (ms)

The present analysis of subdural recordings provided a rare opportunity to check the presence of evoked and induced responses at such an intermediate spatial resolution. We estimated the spatial resolution of our recordings to be on the order of 1 cm, since for subject TY, a rhythmic sequence of epileptic spikes could be observed on a single electrode (9) and not on electrodes only 1 cm away (Le van Quyen *et al*., 1997). A comparison with scalp recordings over the occipital and temporal region (Tallon-Baudry *et al*., 1996) reveals a close correspondence between EEG responses and subdural gamma effects. EEG evoked responses and subdural phase-locking effects were found at the same latencies, based on a comparable phase-alignment detection method. This is also valid for induced gamma responses triggered by stimulations, as both occurred starting at 150 ms, and with similar duration (about 150 ms). In fact, the only major difference between gamma responses at these two recording levels is their spatial distribution, which is more uniform for EEG, as seen for example by the differences detected over a less than 1 cm in response pattern (Fig. 5).

Nevertheless, based on patient TY, EEG and subdural gamma are consistent. A demonstration of a physiological link with microelectrode studies is a further stretch, but a number of animal studies at levels intermediate between microelectrodes and EEG provide some hints (e.g. Bressler *et al*., 1993; Buser & Rougeul-Buser, 1995; König *et al*., 1995; Destexhe *et al*., 1999). Among them, Destexhe *et al*. (1999) suggests a possible mechanism for the formation of the gamma bursts. This study recorded LFPs from area 5 and 7 of awake cats with a millimeter resolution. They observed that spontaneous gamma activity was usually uncorrelated between electrodes separated by more than 2 mm, except for short (a couple of hundreds of milliseconds) episodes during which the spatial correlation extended over more than 5 mm. If gamma activity reproduces this pattern in humans, then it should be largely invisible to intracortical electrodes with a cm spatial resolution, because nonsynchronous local activites would average out over such a surface. However, these electrodes would detect a burst of gamma activity during the short periods of spatial synchronization observed by Desthexhe. We therefore propose that the gamma bursts observed in human intracortical recordings correspond to rapid episodes of spatial synchronization extending over distances of a couple of millimeters.

While there is a good general agreement between our results and the locations of the gamma responses found by Tallon-Baudry *et al*. the latency differences of induced responses were not apparent at the scalp's surface. It seems plausible that these latency differences are blurred by the spatial smearing due to conduction through the head's tissues between cortex and scalp. This also holds for the evoked responses; our results revealed that the phase of the evoked response does not vary with stimulation type. In contrast, this phase depends largely on the electrode's position, so that the evoked response, which appears roughly uniform in surface recordings, is in fact strongly nonuniform at the subdural level, and surely involves a complex system of generators.

Finally, while on the surface Tallon-Baudry *et al*. (1996) found a clear correlation between the level of induced response and the target/nontarget discrimination, this is entirely absent in this study. There are two plausible reasons for this important different. First, we used a simplified protocol as compared to them (the target was a variant of the illusory contour), due to the limitation of working with epileptic patients. It is thus likely that many responses were a simple detection of the component forms, and not the harder identification of an illusory border. Second, the placement of electrodes not being controlled by the protocol, we cannot discard the possibility that the actual choice did not cover more relevant regions. In brief, little can be said of more detailed neurocognitive interpretation, which must await a further study.

A finer-grained picture of evoked and induced responses

Tallon-Baudry *et al*. (1996) could not directly ascertain the anatomical origin from scalp recordings, but assumed that it may have contributions from the visual cortex (striate or extrastriate), hippocampus (based on results from Leung, 1992 and Bragin *et al*., 1995), and/or the cingulate cortex (based on results from Leung & Borst, 1987). This study suggests that, given the diversity in location and delays over the cortex, surface gamma responses are, in fact, a composite of several distributed sources, an important conclusion for their functional interpretation.

In addition, our results on visual discrimination task correspond well to a recent study in intracranial recordings during a visuomotor task (Aoki *et al*., 1999). They recorded from 14 cortical sites in sensorimotor cortex while the subjects performed various motor tasks. They report episodes of gamma oscillations (31–60 Hz) during the execution of certain tasks. Further, different recording sites show differential increases specific to the task, and they are spectrally coherent. Thus our findings here on visual discrimination confirm and complement their observation on sensorimotor activity.

Although we did not record from cingulate cortex, electrodes implantation gave us access to the visual cortex and the hippocampus. For subject BA, energy increases were seen in various parts of the right hippocampus. For subject TY, stimulations induced stronger gamma responses on the occipital side of the occipito-temporal junction, than on the temporal side. In addition, for this subject, induced responses were observed in cortical areas involved in vision (near the parieto-occipital junction and near the antecalcarine sulcus). It has been documented that lesions in the parieto-occipital junction cause Balint's syndrome, which prevents patients from attending two objects at the same time, even if they lie in the same location (Rafal & Robertson, 1995). Energy increases observed in this region may therefore be part of a general object-based attentional processing. This would be in agreement with an increasingly plausible notion that attention may be mediated by the cooperation among selected subpopulations of neurons in widely distributed regions (Posner, 1995).

In conclusion, this study portrays gamma activity in humans as constituted of a patchwork of responses, both evoked or induced, widely distributed in specific brain regions. Following insights provided by animal recordings, the next natural step is to study the possible role of these more detailed oscillations in long-range synchronization, and to determine whether they relate to each other to serve a functional role in cognitive processing as reported from the scalp (Rodriguez *et al*., 1999; Desmedt & Tomberg, 1994; Friston *et al*., 1997). Elsewhere we analyse synchronies between intracranial gamma responses including the introduction of methods to assess their significance (Lachaux *et al*., 1999).

References

Abeles, M. (1991) *Corticonics*, Cambridge University Press, Cambridge, UK.

Aoki, F., Fetz, E.E., Shupe, L., Lettich E., & Ojeman, G.A. (1999) Increased gamma-range activity in human sensori-motor cortex during performance of visuo motor tasks. *Clin. Neurophysiol.*, **110**, 524–537.

Auger, F., Flandrin, P., Goncalves, P. & Lemoine, O. (1995) Time-Frequency Toolbox for use with Matlab. Tutorial. Available at: http://www-syntim.inria.fr/fractals/Software/TFTB/.

Arieli, A., Sterkin, A., Grinvald, A. & Aertsen, A.D. (1996) Dynamics of ongoing activity: Explanation of the large variability in evoked cortical responses. *Science*, **273**, 1868–1871.

Bragin, A., Jando, G., Nadasdy, Z., Hetke, J., Wise, K. & Buszaki, G. (1995) Gamma (40–100 Hz) oscillation in the hippocampus of the behaving rat. *J. Neurosci.*, **15**, 47–60.
Bressler, S.L., Coppola, R. & Nakamura, R. (1993) Episodic multiregional cortical coherence at multiple frequencies during visual task performance. *Nature*, **366**, 153–156.
Bressler, S.L. (1995) Large-scale cortical networks and cognition. *Brain Res. Brain Res. Rev.*, **20**, 288–304.
Buser, P. & Rougeul-Buser, A. (1995) Do cortical and thalamic bioelectric oscillations have a functional role? A brief survey and discussion. *J. Physiologie*, **89**, 249–254.
Damasio, A.R. (1990) Synchronous activation in multiple cortical regions: a mechanism for recall. *Semin. Neurosci.*, **2**, 287–296.
Desmedt, J.E. & Tomberg, C. (1994) Transient phase-locking of 40 Hz electrical oscillations in prefrontal parietal cortex reflects the process of conscious somatic perception. *Neurosci. Lett.*, **168**, 126–129.
Destexhe, A., Contreras, D. & Steriade, M. (1999) Spatiotemporal analysis of local field potentials and unit discharges in cat cerebral cortex during natural wake and sleep states. *J .Neurosci*, **19**, 4595–4608.
Eckorn, R., Frien, A., Bauer, R., Wollbern, T. & Kehr, H. (1993) High frequency (60–90 Hz) oscillations in primary visual cortex of awake monkeys. *Neuroreport*, **4**, 243–246.
Ferster, D. (1996) Is neural noise just a nuisance? *Science*, **273**, 1812.
Flandrin, P. (1993) *Temps-Fréquence. Traité des Nouvelles Technologies, Série Traitement du Signal.* Hermès, Paris.
Freeman, W.J. (1975) *Mass Action in the Nervous System.* Academic Press, New York.
Friston, K.J., Stephan, K.M. & Frackowiak, R.S.J. (1997) Transient phase-locking and dynamic correlations: are they the same thing? *Human Brain Map.*, **5**, 48–57.
Galambos, R., Makeig, S. & Talmachoff, P.J. (1981) A 40 Hz auditory potential recorded from the human scalp. *Proc. Natl Acad. Sci. USA*, **78**, 2643–2647.
Gray, C.M., Konig, P., Engel, A.K. & Singer, W. (1989) Oscillatory responses in cat visual cortex exhibit inter-columnar synchronization which reflects global stimulus properties. *Nature*, **338**, 334–337.
Jokeit, H., Goertz, R., Küchler, E. & Makeig, S. (1994) Event-related changes in the 40-Hz electroencephalogram in auditory and visual reaction time tasks. In Pantev, C., Elbert, T. & Lütkenhöner, B. (eds), *Oscillatory Event-Related Brain Dynamics.* Plenum Press, New York, pp. 135–146.
Kanizsa, G. (1976) Subjective contours. *Sci. Am.*, **235**, 48–52.
König, P., Engel, A.K. & Singer, W. (1995) Relation between oscillatory activity and long-range synchronization in cat visual cortex. *Proc. Natl Acad. Sci. USA*, **92**, 290–294.
Kreiter, A.K. & Singer, W. (1992) Oscillatory neuronal responses in the visual cortex of the awake monkey. *Eur J. Neurosci.*, **4**, 369–375.
Lachaux, J.P., Rodriguez, E., Martinerie J. & Varela, F. (1999) Measuring phase-synchrony in brain signals. *Human Brain Map.* **8**, 194–208.
Le van Quyen, M., Adam, C., Lachaux, J.P., Martinerie, J., Baulac, M., Renault, B. & Varela, F.J. (1997) Temporal patterns in human epileptic activity are modulated by perceptual discriminations. *Neuroreport*, **8**, 1703–1710.
Leung, L.S. (1992) Fast (beta) rhythms in the hippocampus: a review. *Hippocampus*, **2**, 93–98.
Leung, L.S. & Borst, J.G.G. (1987) Electrical activity of the cingulate cortex. I. Generating mechanisms and relations to behavior. *Brain Res.*, **407**, 68–80.
Llinas, R. & Ribary, U. (1993) Coherent 40 Hz oscillation characterizes dream state in humans. *Proc. Natl Acad. Sci. USA*, **90** (5), 2078–2081.
Martin, W. & Flandrin, P. (1983). Analysis of nonstationary processes: short-time periodograms vs. a pseudo-Wigner estimator. In Schüssler, H.W. (ed), *Signal Processing II. Theories and Applications.* North-Holland, Amsterdam. pp. 455–458.
Menon, V., Freeman, W.J., Cutillo, B.A., Desmond, J.E., Ward, M.F., Bressler, S.L., Laxer, K.D., Barbaro, N. & Gevins, A. (1996) Spatio-temporal correlations in human gamma band electrocorticograms. *Electroencephalogr. Clin. Neurophysiol.*, **98**, 89–102.
Neuenschwander, S., Engel, A., König, P., Singer, W. & Varela, F. (1996) Synchronous activity in the optic tectum of awake pigeons. *Vis. Neurosci.*, **13**, 575–584.
Neuenschwander, S. & Varela, F. (1993) Visually triggered oscillations in the pigeon: an autocorrelation study of tectal activity. *Eur. J. Neurosci.*, **5**, 870–881.
Pantev, C., Makeig, S., Hoke, M., Galambos, R., Hampson, S. & Gallen, C. (1991) Human auditory evoked gamma-band magnetic fields. *Proc. Natl Acad. Sci. USA*, **88**, 8996–9000.
Pantev, C. (1995) Evoked and induced Gamma-band activity of the human cortex. *Brain Topog.*, **7**, 321–330.
Perez-Borja, et al. (1961). *Electroencephalogr. Clin. Neurophysiol.*, **13**, 695–702.
Posner, M.I. (1995) Attention in cognitive neuroscience: an overview. In Gazzaniga, M.S. (ed), *The Cognitive Neurosciences*. The MIT Press, Cambridge, London, pp. 615–624
Rafal, R. & Robertson, L. (1995) The neurology of visual attention. In Gazzaniga, M.S. (ed), *The Cognitive Neurosciences*. The MIT Press, Cambridge, London, pp. 625–649.
Ribary, U., Ioannides, A.A., Singh, K.D., Hasson, R., Bolton, J.P.R., Lado, F., Mogilner, A. & Llinas, R. (1991) Magnetic field tomography of coherent thalamocortical 40-Hz oscillations in humans. *Proc. Natl Acad. Sci. USA*, **88**, 11037–11041.
Rodriguez, E., George, N., Lachaux, J.P., Matrincrie, J., Renault, B. & Varcla, F.J. (1999) Perception's shadow: long-distance synchronization of human brain activity. *Nature*, **397**, 430–433.
Roelfsema, P.R., Engel, A.K., König, P. & Singer, W. (1997) Visuomotor integration is associated with zero time-lag synchronization among cortical areas. *Nature*, **385**, 157–161.
Schürman, M., Basar-Eroglu, C. & Basar, E. (1997) Gamma-responses in the EEG: elementary signals with multiple functional correlates. *Neuroreport.*, **8**, 1793–1796.
Singer, W. & Gray, C.M. (1995) Visual feature integration and the temporal correlation hypothesis. *Annu. Rev. Neurosci.*, **18**, 555–586.
Tallon, C., Bertrand, O., Bouchet, P. & Pernier, J. (1995) Gamma-range activity evoked by coherent visual stimuli in humans. *Eur. J. Neurosci.*, **7**, 1285–1291.
Tallon-Baudry, C., Bertrand, O., Delpuech, C. & Pernier, J. (1996) Stimulus specificity of phase-loked and non-phase-locked 40 Hz visual responses in human. *J. Neurosci.*, **16**, 4240–4249.
Tallon-Baudry, C., Bertrand, O., Delpuech, C. & Pernier, J. (1997) Oscillatory gamma-band (30–70 Hz) activity induced by a visual search task in human. *J. Neurosci.*, **17**, 722–734.
Tallon-Baudry & Bertrand (1999) Oscillatory gamma activity in humans and its role in object representation. *Trends Cognit. Sci.*, **3**, 151–162.
Theiler, J., Eubank, S., Longtin, A., Galdrikian, B. & Farmer, J.D. (1992) Testing for non-linearities in time series: The method of surrogate data. *Physica D.*, **58**, 77–94.
Varela, F.J. (1995) Resonant cell assemblies: a new approach to cognitive functions and neuronal synchrony. *Biol. Res.*, **28**, 81–95.

Appendix I. The Wigner–Ville Transform

The smoothed-pseudo-Wigner–Ville (PWV) estimates the energy present in a signal x around a time t and a frequency f as:

$$PWV(f,t) = \int_{-\infty}^{+\infty} |h(\tau/2)|^2 \left[\int_{-\infty}^{+\infty} g(u-t)x(u-\tau/2)x^*(u-\tau/2)du\right] cos(2\pi f\tau)d\tau.$$

This formula is derived from the original definition of the Wigner–Ville transform to which two smoothing functions have been added: h is a short-term observation window used for frequency smoothing (in this study, a Hamming window of length 128 ms), and g is a temporal smoothing window (the same as h in this study). The complex conjugate of $x(t)$ is indicated by x^*.

The purpose of these smoothing functions is to minimize interference, a common limitation of the original Wigner–Ville transform. Because it is nonlinear, the Wigner–Ville transform of the sum of two signals is not exactly the sum of the Wigner–Villes of each individual signal. The nonlinearity adds a spurious term referred

to broadly as 'interference'. An easy way to think of these interference is to imagine an EEG signal with two oscillatory bursts: a first burst around 10 Hz occurring at 100 ms and a second burst around 30 Hz at 300 ms. This signal can also been thought of as the sum of two signals, each of them containing one of the bursts. The ideal time-frequency description of the 'two-bursts' signal would contain only two blobs of energy, one at (10 Hz, 100 ms) and one at (30 Hz, 300 ms). This ideal description matches the sum of the Wigner–Ville transforms of the two 'single-burst' EEG signals. But since the Wigner–Ville transform is nonlinear, the actual Wigner–Ville map of the 'two-bursts' signal will have, in addition to the two blobs, an extra-blob, or interference, at their geometric midpoint (20 Hz, 200 ms) with a fraction of the energy of the main blobservation

In this study, interference were minimized by eliminating the high energies of the low frequencies (high-pass filtering) and by using the smoothed-pseudo Wigner–Ville instead of the original Wigner–Ville transform (Martin & Flandrin, 1983; Auger *et al*., 1995).

Appendix II. Time-frequency charts of emission

To obtain the time-frequency charts shown in Fig. 5 the following procedure was followed: (i) For each trial, we computed the Wigner time-frequency map $E(t,f)$ of the raw signal (unfiltered); (ii) for each frequency f_i, we computed the mean (m) and standard deviation (σ) of the energy measured before stimulation $E[(-400\text{ ms}, -50\text{ ms}), f_i]$, and computed $E'(t, f_i) = [E(t, f_i) - m]/\sigma$ (z-score baseline correction). By construction, the portion of the time-frequency map $E'(t,f)$ preceding the stimulation has a zero mean and a standard deviation of 1 before stimulation. Thus, $E'(t,f)$ is the energy increase at time t relative to baseline for a given frequency f; and (iii), finally, we averaged all maps E' across trials in order to obtain the maps shown in this figure. All scales are linear, and the white horizontal line indicates intermediate frequency $f = 40$ Hz as a visual aid. A key advantage of this procedure is that results can be compared to scalp data similarly analysed by Tallon-Baudry *et al*. (1996) in a comparable task (see Discussion).